Continuously tunable super-efficient microcombs

Research Article Vol. 34, No. 6 / 23 Mar 2026 / Optics Express 9669
Optics EXPRESS

Continuously tunable super-efficient microcombs

ISRAEL REBOLLEDO-SALGADO,[1,*] NIKLAS HAMMERSCHMIDT,[1,2] TIM FUHRMANN,[2] CARMEN H. LÓPEZ-ORTEGA,[2] MARTIN ZELAN,[1] AND VICTOR TORRES-COMPANY[2]

[1]*Measurement Science and Technology, RISE Research Institutes of Sweden, SE-501 15 Borås, Sweden*
[2]*Department of Microtechnology and Nanoscience (MC2), Photonics Laboratory, Chalmers University of Technology, SE-412 96 Gothenburg, Sweden*
[*]*israel.rebolledo@ri.se*

Abstract: Microcombs are steadily advancing toward system-level applications. Recent progress in high-Q silicon nitride microresonators and coupled cavities allows for generating coherent microcombs with an optical conversion efficiency approaching unity. The generation of efficient soliton microcombs in this coupled cavity arrangement (photonic molecule) relies on controlling the strength and location of an avoided mode crossing to compensate for the spectral shift introduced by the temporal soliton. While resulting in exceptionally high efficiency and reliability, it is challenging to attain continuous broadband tuning of the pump, limiting deployment in some practical applications. In this work, we demonstrate offset-tunable super-efficient microcombs in photonic molecules featuring low-noise operation and a smooth, constant spectral envelope. This is achieved by thermally tuning in tandem the main and auxiliary cavities, allowing to attain the desired avoided mode crossing across multiple free spectral ranges of the main cavity. Additionally, we analyze the impact of the thermal tuning on the phase noise and repetition rate stability as well as the thermal response of heaters. The demonstrated broadband, post fabrication tunability establishes photonic molecules as a highly flexible and efficient platform for the generation of super-efficient microcombs at arbitrary pump wavelengths, making this configuration a particularly appealing one for applications in metrology and precision spectroscopy.

1. Introduction

Over the past two decades, the development of chip-scale frequency combs has undergone remarkable advancements, largely by leveraging the progress in integrated photonics [1]. The field has now advanced well beyond the initial demonstrations of mode-locked soliton states in microcavities [2] and is rapidly moving towards system-level applications that exploit the bandwidth [3], coherence [4], and mode spacing [5] attainable with microcombs. At the same time, there have been major efforts to bring these systems outside the laboratory, including packaging [6,7], long-term stabilization [8–10], and low-power consumption [11,12].

Most of these demonstrations have focused on using dissipative Kerr solitons (DKSs) generated in a single microcavity [13]. By counterbalancing the anomalous dispersion of the microresonator with the Kerr nonlinearity, the DKS features a smooth sech profile in both time and frequency domains. The detuning required to operate the DKS results in a low conversion efficiency of the microcomb, where only a small fraction of the pump laser is converted into useful comb lines [2,13].

Alternative microcomb states and configurations have been investigated to achieve higher conversion efficiency, including soliton crystals [14,15], pulse pumping [16–18], normal-dispersion

#587631 https://doi.org/10.1364/OE.587631
Journal © 2026 Received 15 Dec 2025; revised 24 Jan 2026; accepted 27 Jan 2026; published 10 Mar 2026

Optics EXPRESS

cavities [19–22], and selective pumping at avoided mode crossings (AMCs). Deterministic generation control under continuous-wave (CW) pumping requires precise engineering of the AMCs, which can be implemented using photonic crystal resonators [23,24] or through two coupled cavities, i.e., photonic molecules [25–27].

In addition to high conversion efficiency, another key feature for practical applications is the ability to continuously tune the pump wavelength over a broad spectral range. Enhanced control over the offset frequency of the microcomb has enable applications such as tunable spectroscopy [28], frequency-modulated LiDAR [29], and fast-feedback control loops for phase stabilization [9,30]. Although such tunability has been demonstrated using normal-dispersion microcombs [25], it remains a significant challenge for photonic molecule microcombs relying on integrated heaters [10,31,32] or piezoelectric actuators [33,34].

In this work, we overcome this limitation and demonstrate that the pump wavelength of super-efficient microcombs can be tuned continuously over a broad bandwidth. This is achieved by exploiting the photonic molecule architecture, in which the engineered AMC selected for pumping is thermally tuned across spectral regions previously inaccessible due to its fixed position after fabrication. Our method leverages the two degrees of freedom inherent to the photonic molecule to generate super-efficient microcombs, by jointly tuning the main and auxiliary cavities, the pumped resonance is tuned across the free spectral range (FSR) of the main cavity. Then, by tuning the auxiliary cavity over its own FSR, the AMC itself is shifted, allowing access to consecutive longitudinal modes of the main cavity for pumping. Here, we tuned the pump across nearly four times the microcomb's repetition rate, however, due to the Vernier effect between the cavities, this approach can in principle enable tuning to any spectral location within the microcomb's bandwidth.

These results highlight the versatility of thermal tuning in photonic molecules, enabling the generation of highly efficient microcombs at arbitrary pump wavelengths, a capability of particular relevance for metrology and precision spectroscopy, where locking to specific optical references and high-resolution measurements are required.

2. Discrete tuning of high-efficient microcombs

The photonic molecule used in the following experiments comprises an arrangement of two cavities with anomalous dispersion, main and auxiliary, that has a large mismatch in their FSRs (see Fig. 1(a)). This mismatch induces a selective shift of the pump resonance, allowing an anomalous-dispersion soliton to operate with the pump laser close to resonance, therefore, achieving high power-conversion efficiencies [10,32,35]. Nevertheless, choosing this arrangement minimizes the interaction of the auxiliary cavity with adjacent longitudinal modes of the main cavity, which makes them unsuitable for pumping.

Previous works have exploited the thermo-optic effect in silicon nitride resonators through integrated microheaters, enabling tunable mode splitting and improved comb generation [25,26,36,37]. By leveraging the thermo-optic effect, we tune the AMC over the FSR of both the main and auxiliary cavities, as illustrated in in Fig. 1(b). In the first set of experiments, we linearly increase the electrical power applied to the main cavity heater to tune the microcomb across its repetition rate. Using the same approach on the auxiliary cavity, we further shift the AMC, allowing us to access consecutive longitudinal modes of the main cavity. By combining these two tuning mechanisms over their respective FSRs, we achieved continuous tunability of the pump wavelength.

The photonic molecule used in this study is contained in a $5 \times 5\,\mathrm{mm}^2$ chip, which is part of a range of silicon nitride (Si_3N_4) photonic devices reported in [35]. A microheater is integrated on top of the upper cladding of each resonator by depositing a 200-nm-thick platinum layer with a 5-nm titanium adhesion layer. The heaters are separated from the microrings by a 3-μm-thick SiO_2 buffer layer, which suppresses metal-induced optical absorption while preserving the modal

Optics EXPRESS

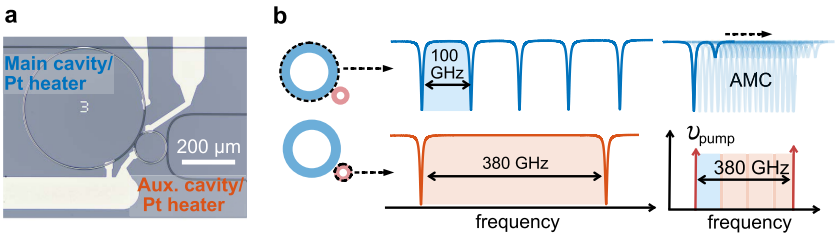

Fig. 1. Continuously tunable super-efficient microcombs. (a) Microscope picture of the photonic molecule with the platinum. (Pt) heaters on top of the main and auxiliary cavity. (b) The photonic molecule provides two tuning degrees of freedom of the avoided mode crossing (AMC), by jointly tuning the main and auxiliary cavities the microcomb is offset tuned across its repetition rate, while tuning only the auxiliary cavity shifts the AMC to access consecutive longitudinal modes, allowing a continuous tunability of the pump wavelength.

properties of the resonators. Figure 2(a) shows finite-element method (FEM) simulations of the propagation loss and group index as a function of the cladding thickness. The simulations indicate that the propagation loss decreases rapidly with increasing oxide thickness and reaches a minimum for thicknesses exceeding approximately 2.5 μm, confirming that the optical mode is sufficiently isolated from the metal heater for the chosen geometry. In addition, the group index remains effectively constant over this cladding-thickness range, indicating that the presence of the heater and buffer layer does not result in a measurable change of the cavity free spectral range.

The platinum heaters are deposited by electron-beam evaporation. The measured electrical resistance at the contact pads is 126 Ω for the main heater and 47 Ω for the auxiliary heater. The microheaters are placed directly on top of each microring resonator and have lengths of approximately 1.19 mm and 314 μm for the main and auxiliary cavities, respectively, with an additional routing section of approximately 1.68 mm used to connect the heaters to the electrical probe pads at the chip edge.

The photonic molecule was characterized using swept-wavelength interferometry with self-referenced frequency comb calibration [38]. The main cavity has a radius of 227.8 μm, corresponding to a free spectral range (FSR) of 99.69 GHz. The auxiliary cavity has a radius of 60 μm, corresponding to an FSR of 380 GHz. The measured mean intrinsic and extrinsic quality factors of the main cavity are Q_i = 9.7 million and Q_e = 1.7 million, respectively. The gap between the rings is 500 nm, while the gap between the main cavity and the bus waveguide is 300 nm. The coupled resonators have the same cross-section dimensions of 1800 nm width and 740 nm height. This waveguide geometry exhibits anomalous dispersion in the telecom C-band. The measured dispersion in the main cavity corresponds to $-80\,\mathrm{ps}^2/\mathrm{km}$ at 1550 nm.

The coupling between the microresonators results in the shift of a specific mode in the main cavity. By bringing the auxiliary resonance into close proximity with the main resonance using the heaters, the mode splitting is finely controlled. The microcombs are then generated by pumping a hybridized resonance in a photonic molecule. To generate a single DKS, the laser is tuned from the blue towards the red, followed by fine-tuning of the auxiliary cavity resonance using the integrated heaters. A conversion efficiency higher than 50% is obtained by reducing the pump power, as described in [10,32].

The setup for the microcombs generation and thermal tuning is show in Fig. 2(b). The chip is placed in a thermally stabilized stage with a temperature stability of 20 mK (over 24 hours) measured at the stage sensor. A continuous-wave external-cavity diode laser (ECDL) is coupled through lensed fibers to the bus waveguide of the photonic molecule. The on-chip optical power used for pumping the device is 14 dBm. A fiber Bragg grating (FBG) filter is used during the initiation process to monitor the pump and soliton-converted powers using two photodetectors.

Optics EXPRESS

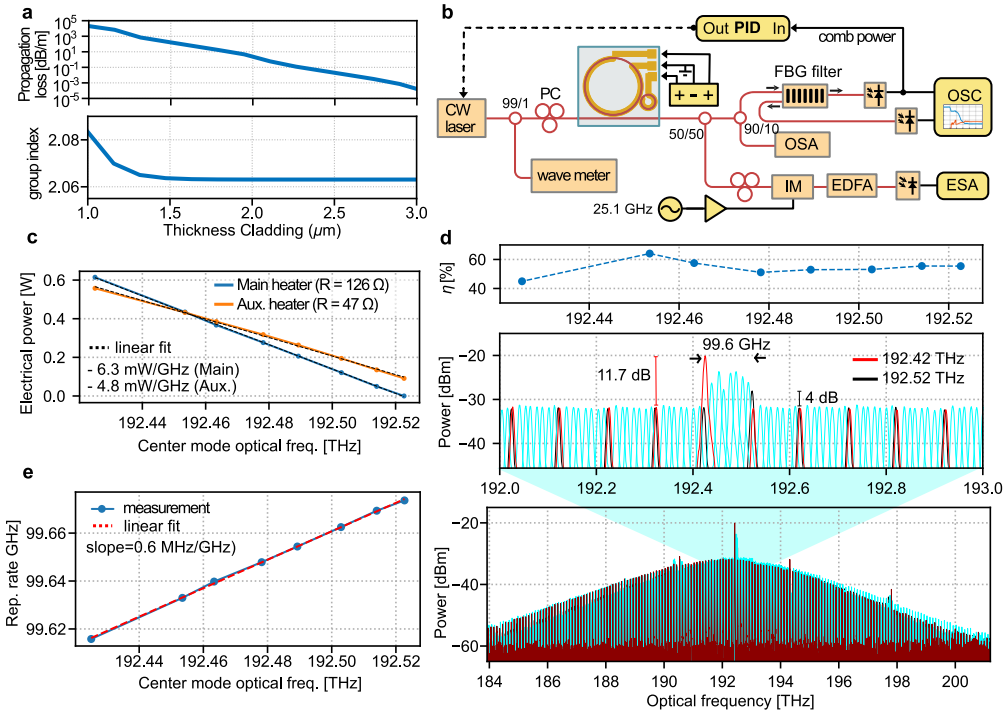

Fig. 2. Tuning of a super-efficient microcomb over its repetition rate. (a) Finite-element method simulation of the waveguide showing the dependence of propagation loss and the group index with respect to the cladding thickness. (b) Experimental setup for generation of a soliton and the characterization of the repetition rate through electro-optic down-conversion. PC Polarization controller, FBG Fiber-Bragg Grating, OSA Optical Spectrum Analyzer, IM Intensity Modulator, EDFA Erbium-doped fiber amplifier, ESA Electrical Spectrum Analyzer, OSC Oscilloscope. (c) Characterization of the electrical power required to tune the central pump frequency over 100 GHz. (d) Comb spectra as the pump laser is tuned over the microcomb repetition rate (99.6 GHz). A power conversion efficiency (η) of 54% (in average) is maintained throughout the tuning, as evidenced by the suppression of the central pump line and the corresponding variations in the microcomb bandwidth. (e) Variation of the repetition rate with respect to the pump frequency.

Optics EXPRESS

The microcomb optical power, with the pump filtered out, is split into different branches to characterize its optical spectrum and repetition rate [39]. The photodetected soliton power is also used as a setpoint for a proportional–integral–derivative (PID) controller, which generates a feedback signal for the pump laser piezocontroller [10].

The feedback control loop is implemented to assist in the generation of the super-efficient microcomb and to streamline the tuning of the pump wavelength. Although microcomb generation can be achieved by tuning only the auxiliary resonance together with the laser frequency, as demonstrated in [32], including an automated feedback control significantly improves the speed and reproducibility of the generation process. During microcomb generation, the FBG filter remains fixed. However, during tuning, the center wavelength of the FBG filter is manually adjusted to track the pump laser frequency. This prevents residual pump power from leaking into the soliton power signal used by the PID controller, which would otherwise degrade the feedback resolution. With this approach, the generated microcombs maintain a consistent spectral shape and power by preserving a constant soliton power across the tuning range.

To offset tune the microcomb over its repetition rate, a single avoided mode crossing is tuned within one full FSR of the main cavity (0.82 nm), leveraging the thermo-refractive effect [25,26] by setting the voltages on the integrated microheaters using a DC power supply. A first characterization of the heaters tuning efficiency is shown in Fig. 2(c), resulting in efficiencies of 1.33 nm/W (6.3 mW/GHz) and 1.5 nm/W (4.8 mW/GHz) for the main and auxiliary heater, respectively. The observed difference in tuning efficiency can be attributed to a larger effective temperature change experienced by the optical mode, rather than a direct dependence on heater length [25]. The microcombs are then generated by tuning the AMC in steps of 0.1 nm by applying the required electrical power to the main and auxiliary ring heaters and consecutively pumping with the ECDL while monitoring its wavelength using a wavemeter. The recorded set of optical spectra is shown in Fig. 2(d), for pump wavelengths ranging from 1557.18 nm to 1557.98 nm (black traces). To verify the formation of a low-noise, phase-locked state, the microcomb was sent to a photodiode connected to an electrical spectrum analyzer (ESA) to monitor the absence of low-frequency components.

The optical conversion efficiency (CE), given by the ratio of the output comb power (without the pump) divided by the pump power was characterized at each pump wavelength. The highest conversion efficiency obtained was 64% at 1557.5 nm while the lowest CE found corresponds to 45% at 1557.98 nm. As shown in Fig. 2(d), the spectral envelope experiences minor changes while tuning across the repetition rate. The optical bandwidth is observed to increase at certain pump wavelengths, allowing a higher CE despite the pump power was not reduced as much as in the other cases. For this case, the soliton power increased and therefore the setpoint used to control the laser, which indicates a different detuning than for the rest of the pump wavelengths.

The repetition rate (f_{rep}) of the microcombs was characterized using an electro-optic down-conversion using a low phase noise RF oscillator with a frequency of 25.1 GHz [39]. The change of f_{rep} versus pump frequency is shown in Fig. 2(e). The measurements are fitted with a linear function and a slope of 0.59 MHz/GHz is inferred. This tuning efficiency is of the same order as previously reported thermal tuning responses [25] and is mainly attributed to thermally induced changes in the cavity refractive index and optical path length as the pump frequency varies. The observed shift is notably larger than the change expected from pump–resonance detuning alone, indicating that thermal effects dominate the repetition rate variation [40]. Although both detuning and thermal perturbations can degrade repetition-rate stability, detuning fluctuations can be compensated through soliton power control [9,10], and the resonator temperature can be effectively stabilized using an integrated thermometer with active compensation [41]. In the soliton regime, an additional contribution to f_{rep} can arise from the soliton self-frequency shift due to the Raman effect [42,43], although our simulations using our experimental parameters indicate that this dependence is weak, introducing only a few-kilohertz variation.

Optics EXPRESS

To investigate how the temperature increase in the photonic molecule affects the stability of the high-efficiency microcombs, the phase noise of the down-converted repetition rate was measured. The single-sideband (SSB) phase noise curves and the beat notes recorded for every microcomb are shown in Fig. 3(a) and (b), respectively. As the electrical power applied to the heaters increases, the phase noise increases, and a broadening of the linewidth of the repetition rate beat note is visible. Previous works have shown that thermal noise imposes a fundamental decoherence mechanism in micro-cavities, arising from thermo-refractive fluctuations of the refractive index and thermal expansion of the cavity [44–46].

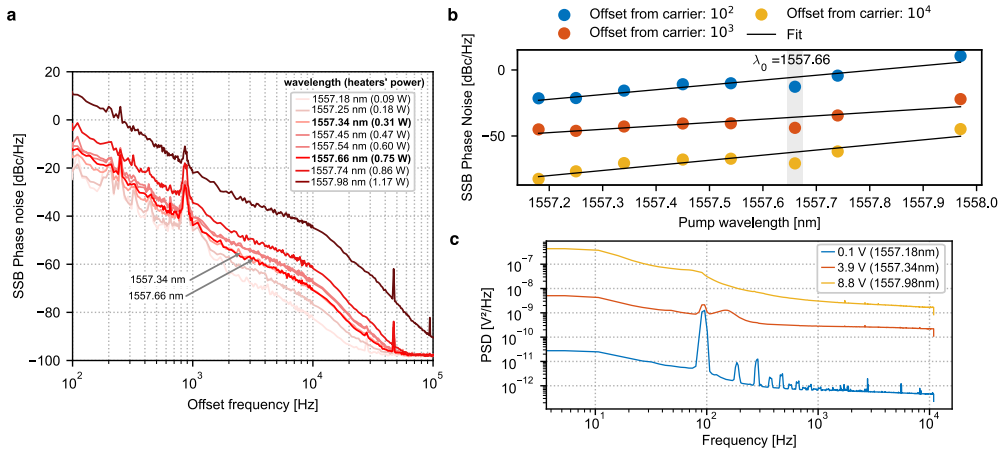

Fig. 3. Electrical phase noise of the repetition rate. (a) Single sideband (SSB) phase noise of the down-converted repetition rate while tuning the microcomb. (b) Phase noise values at selected offset frequencies for the generated microcombs. While the values generally exhibit an almost linear increase, a deviation from this trend is observed at 1557.66 nm, where the phase noise decreases. (c) Power spectral density for three output voltages of the power supply used to tune the microcomb.

In our measurements, an increase in heater power elevates the absolute temperature of the resonator, which in turn amplifies intrinsic temperature fluctuations and enhances their conversion into phase noise through changes in the optical path length and effective refractive index. Using the thermal tuning coefficient reported in [25] (2.63 GHz/°C for the center frequency tuning), the measured shift of 97.62 GHz corresponds to a temperature rise of approximately 37°C.

The phase noise degradation can also be attributed to the increased electronic noise in the tuning circuit, in specific, the power supply. Figure 3(c) shows the voltage-noise spectral densities measured directly at the output of the power supply for three different output voltages. This explains the correlated increase in phase noise and linewidth broadening of the repetition rate beat notes with the increase in the heater power.

Interestingly, a reduction in phase noise is observed at 1557.66 nm which overlaps with the phase noise of the initial pump wavelength of 1557.34 nm, despite a 0.25 W difference in heater power applied to the main cavity. The SSB phase noise at three selected offset frequencies of the repetition rate is shown in Fig. 3(b), highlighting the reduction observed at 1557.6 nm. This behavior can be attributed to the presence of a quiet point at a specific detuning of that pump wavelength, as previously reported in single cavities with anomalous dispersion [47,48], as well as in photonic molecules operating in both the normal [49] and anomalous dispersion regimes [50]. A more detailed characterization of this effect is left for future work.

Optics EXPRESS

3. Broadband tuning of the avoided mode-crossing

Due to the large mismatch between the main and auxiliary cavities required to shift a single mode of the main cavity, the avoided mode crossings available for pumping are separated by several FSRs of the main cavity. This separation is dictated by the FSR of the auxiliary cavity, which is nearly four times larger than the main cavity one. As shown in the previous section, microcombs with high conversion efficiency can be generated at any pump frequency within one main-cavity FSR. In a second set of experiments, we investigate the feasibility of tuning the spectral position of the auxiliary resonance across its own FSR. This approach enables tuning of the spectral location of the shifted resonance, thereby allowing microcomb generation at spectral regions that would otherwise be inaccessible due to the fixed position of the AMC.

Figure 4(a) illustrates the spectral tuning of the AMC, where its location is shifted from 1557.18 nm to 1559.91 nm, corresponding to 340 GHz, near the 90% of the auxiliary cavity FSR. This tuning is achieved solely by varying the voltage applied to the auxiliary heater, while keeping the main cavity heater fixed, requiring a total power of 1.8 W. The coupling strength between the rings across the spectral locations of the shifted avoided mode-crossing is measured as $\kappa/2\pi = 1.1$ GHz.

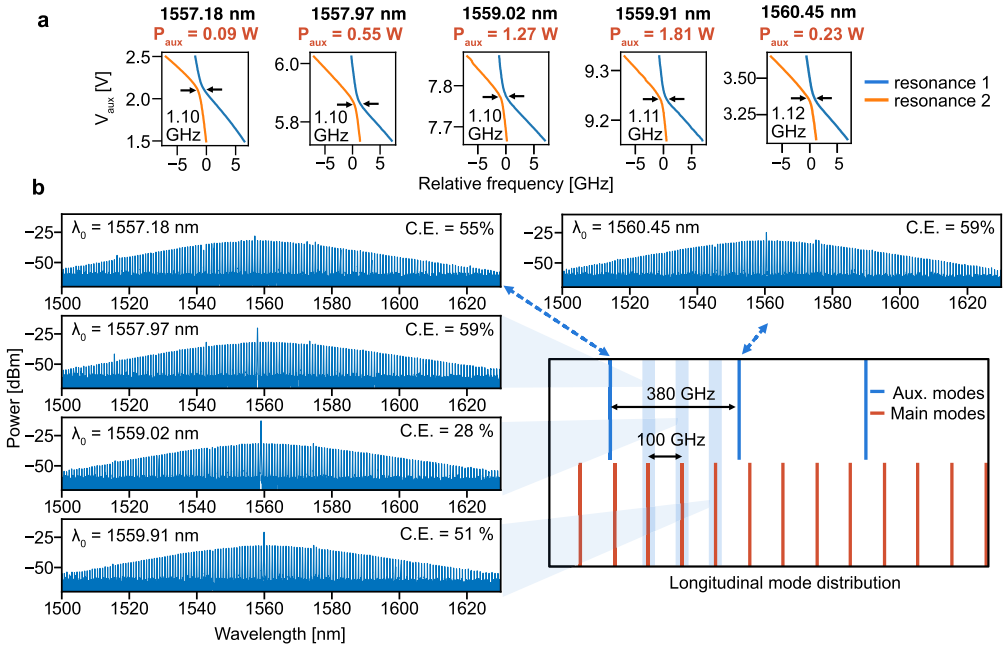

Fig. 4. Tuning of the auxiliary cavity over its free-spectral range. (a) Transmission spectra as a function of the voltage applied to the auxiliary heater to induce the avoided mode crossings (AMC) at every mode of the main cavity. (b) Microcombs generated by pumping the shifted AMC.

The shifted resonances are then pumped to generate high-efficiency microcombs following the same procedure described in the previous section. For microcomb generation, the pump laser frequency and the auxiliary cavity resonance are tuned sequentially to reach the soliton state. After soliton formation, the input optical power is gradually reduced to maximize the conversion efficiency. Since this process directly modifies the detuning between the pump laser and the hybridized resonance, a feedback control loop is employed to stabilize the soliton power and ensure smooth and reproducible operation. The corresponding optical spectra are

Optics EXPRESS

shown in Fig. 4(b). Due to fabrication-induced geometrical variations, an initial fine tuning of approximately 20 GHz (requiring 0.09 W, see Fig. 2(c)) is necessary to reach the first main resonance. By further tuning the auxiliary cavity, adjacent resonances of the main cavity can be accessed. After tuning across three FSRs of the main cavity, the applied voltage approached the maximum output of the low-noise DC supply used for this experiment. Nevertheless, since the tuning covers 90 % of the auxiliary cavity FSR, the shifted AMC aligns closely with the one induced by the consecutive auxiliary resonance mode. At this point, the heater power is reduced, and the next non shifted AMC is employed to generate the microcomb at 1560.45 nm.

The conversion efficiency remained consistently within a two-digit range: all microcombs maintained efficiencies above 50 %, with the exception of the comb at 1559.02 nm, which reached only 28%. We also analyzed the phase noise of the down-converted repetition rate. As expected, the phase noise increases with higher electrical power applied to the heaters. Reducing the pump power to the second auxiliary microcavity (AMC) lowers the phase noise to a level slightly above that of the initial AMC at 1557.18 nm, due to the need to slightly retune the auxiliary resonance. Overall, the trend of increasing phase noise with heater tuning is consistent across different offset-frequency decades when the main cavity heater is adjusted.

The procedure described can be repeated recursively, increasing the electrical power to tune the second AMC until the next auxiliary cavity mode is reached. Combined with the ability to tune the main cavity FSR, this demonstrates the feasibility of generating high-efficiency microcombs at any desired wavelength within the telecom bands.

4. Thermal response time of the heaters

In our configuration, for the generation, stabilization, and tuning of the microcombs, the platinum heater serves as the primary actuator. Therefore, a time-domain characterization of the micro-heater is of significant interest. The setup used for this characterization is illustrated in Fig. 5(a). A continuous-wave laser is coupled to the main cavity at low optical power to minimize thermal instabilities due to self-heating [51]. The micro-heater is driven by a rectangular waveform generated by a signal generator, which induces a modulation of the optical power in the microring through the thermo-optic effect [25,36]. The laser wavelength is carefully set at one edge of the resonance using the laser's piezo controller. It is important that both the laser position and the amplitude of the rectangular waveform are chosen to operate within the linear region of the resonance. In this experiment, the waveform voltage peak-to-peak was set to 0.5 V.

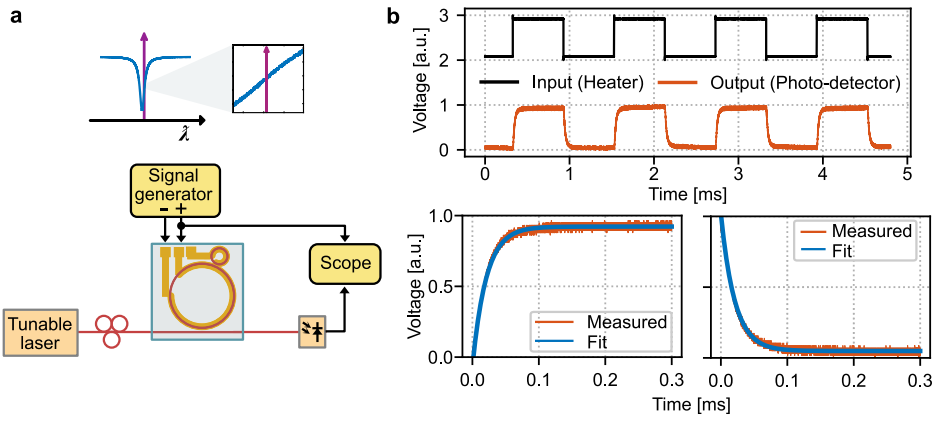

Fig. 5. (a) Setup for measuring the thermal response time. (b) Voltage applied on the microheater and the recorded response of the photodetector. (c) Measured and fitted of the rising and falling edge at the output of the photodetector.

Optics EXPRESS

The optical response is recorded using a photodetector, simultaneously with the signal applied to the heater, via an oscilloscope (see Fig. 5(b)). The thermal response time is then determined by fitting an exponential function to the rising and falling edges, as shown in Fig. 5(c). The time constants extracted from this fitting are 20.86 μs and 20.84 μs for the rising and falling edges, respectively, indicating that the heating and cooling responses are nearly identical. Based on the measured rise and settling times, and assuming a first-order system, the estimated bandwidth of the heater corresponds to 16.78 kHz. These results suggest that a closed-loop controller can be readily implemented using simple feedback circuitry, such as those available on embedded FPGA boards [10,52].

5. Summary

We have demonstrated continuously tunable, high-efficiency microcombs in a photonic molecule architecture by thermally tuning engineered avoided mode crossings over a large bandwidth. By jointly controlling the main and auxiliary cavity resonances, we accessed consecutive longitudinal modes of the main cavity while maintaining low-noise, phase-locked states and conversion efficiencies consistently above 50 per cent. The tuning preserved smooth spectral envelopes and allowed precise control of the repetition rate, with phase-noise measurements indicating increases at higher heater powers due to a combination of thermal fluctuations and electronic noise.

This approach addresses the limitations of fixed cavity resonances suitable for pumping and the inherent large repetition rate of microcombs enabling post-fabrication flexibility and continuous access to pump wavelengths over a broad bandwidth. By addressing these limitations, this work paves the way for the implementation of super-efficient microcombs in practical applications such as high-resolution spectroscopy and precision metrology.

Looking forward, replacing thermo-optic heaters with piezoelectric (PZT) actuators could dramatically reduce power consumption and mitigate thermally induced phase-noise, further enhancing microcomb stability. Combined with low-noise, high-bandwidth electronics, such advancements will lead towards fully integrated, energy-efficient microcomb systems capable of meeting the stringent requirements of real-world applications.

Funding. Horizon Europe (MSCA DN MicrocombSys (GA 101119968)); Swedish Research Council (VR 2020-00453); Swedish Foundation for Strategic Research (FID22-0025); VINNOVA (2024-03559, Vinnova Metrology Programme).

Acknowledgment. The Si_3N_4 devices were fabricated at Myfab Chalmers.

Disclosures. Victor Torres-Company is co-founder and shareholder of Solinide Photonics AB.

Data availability. Data underlying the results presented are available in Ref. [53].

References

1. L. Chang, S. Liu, and J. E. Bowers, "Integrated optical frequency comb technologies," Nat. Photonics **16**(2), 95–108 (2022).
2. T. Herr, V. Brasch, J. D. Jost, *et al.*, "Temporal solitons in optical microresonators," Nat. Photonics **8**(2), 145–152 (2014).
3. K. Wu, N. P. O'Malley, S. Fatema, *et al.*, "Vernier microcombs for integrated optical atomic clocks," Nat. Photonics **19**(4), 400–406 (2025).
4. A. A. Jørgensen, D. Kong, M. R. Henriksen, *et al.*, "Petabit-per-second data transmission using a chip-scale microcomb ring resonator source," Nat. Photonics **16**(11), 798–802 (2022).
5. M. Ludwig, F. Ayhan, T. M. Schmidt, *et al.*, "Ultraviolet astronomical spectrograph calibration with laser frequency combs from nanophotonic lithium niobate waveguides," Nat. Commun. **15**(1), 7614 (2024).
6. A. S. Raja, J. Liu, N. Volet, *et al.*, "Packaged photonic chip-based soliton microcomb using an ultralow-noise laser," arXiv (2019).
7. N. Y. Dmitriev, S. N. Koptyaev, A. S. Voloshin, *et al.*, "Hybrid integrated dual-microcomb source," Phys. Rev. Appl. **18**(3), 034068 (2022).
8. Y. Geng, W. Cui, J. Sun, *et al.*, "Enhancing the long-term stability of dissipative kerr soliton microcomb," Opt. Lett. **45**(18), 5073–5076 (2020).
9. X. Yi, Q.-F. Yang, K. Y. Yang, *et al.*, "Active capture and stabilization of temporal solitons in microresonators," Opt. Lett. **41**(9), 2037–2040 (2016).

Optics EXPRESS

10. I. Rebolledo-Salgado, Ó. B. Helgason, V. Durán, *et al.*, "Active feedback stabilization of super-efficient microcombs in photonic molecules," Opt. Lett. **49**(9), 2325–2328 (2024).
11. J. Liu, A. S. Raja, M. Karpov, *et al.*, "Ultralow-power chip-based soliton microcombs for photonic integration," Optica **5**(10), 1347–1353 (2018).
12. C. Xiang, J. Liu, J. Guo, *et al.*, "Laser soliton microcombs heterogeneously integrated on silicon," Science **373**(6550), 99–103 (2021).
13. T. J. Kippenberg, A. L. Gaeta, M. Lipson, *et al.*, "Dissipative Kerr solitons in optical microresonators," Science **361**(6402), eaan8083 (2018).
14. D. C. Cole, E. S. Lamb, P. Del'Haye, *et al.*, "Soliton crystals in kerr resonators," Nat. Photonics **11**(10), 671–676 (2017).
15. M. Karpov, M. H. Pfeiffer, H. Guo, *et al.*, "Dynamics of soliton crystals in optical microresonators," Nat. Phys. **15**(10), 1071–1077 (2019).
16. E. Obrzud, S. Lecomte, and T. Herr, "Temporal solitons in microresonators driven by optical pulses," Nat. Photonics **11**(9), 600–607 (2017).
17. E. Obrzud, M. Rainer, A. Harutyunyan, *et al.*, "A microphotonic astrocomb," Nat. Photonics **13**(1), 31–35 (2019).
18. M. Rowley, P.-H. Hanzard, A. Cutrona, *et al.*, "Self-emergence of robust solitons in a microcavity," Nature **608**(7922), 303–309 (2022).
19. X. Xue, Y. Xuan, Y. Liu, *et al.*, "Mode-locked dark pulse Kerr combs in normal-dispersion microresonators," Nat. Photonics **9**(9), 594–600 (2015).
20. S.-W. Huang, H. Zhou, J. Yang, *et al.*, "Mode-locked ultrashort pulse generation from on-chip normal dispersion microresonators," Phys. Rev. Lett. **114**(5), 053901 (2015).
21. B. Y. Kim, Y. Okawachi, J. K. Jang, *et al.*, "Turn-key, high-efficiency Kerr comb source," Opt. Lett. **44**(18), 4475–4478 (2019).
22. A. Fülöp, M. Mazur, A. Lorences-Riesgo, *et al.*, "High-order coherent communications using mode-locked dark-pulse Kerr combs from microresonators," Nat. Commun. **9**(1), 1598 (2018).
23. S.-P. Yu, E. Lucas, J. Zang, *et al.*, "A continuum of bright and dark-pulse states in a photonic-crystal resonator," Nat. Commun. **13**(1), 3134 (2022).
24. A. E. Ulanov, T. Wildi, N. G. Pavlov, *et al.*, "Synthetic reflection self-injection-locked microcombs," Nat. Photonics **18**(3), 294–299 (2024).
25. X. Xue, Y. Xuan, C. Wang, *et al.*, "Thermal tuning of kerr frequency combs in silicon nitride microring resonators," Opt. Express **24**(1), 687–698 (2016).
26. S. A. Miller, Y. Okawachi, S. Ramelow, *et al.*, "Tunable frequency combs based on dual microring resonators," Opt. Express **23**(16), 21527–21540 (2015).
27. B. H. Óskar, A. Fülöp, J. Schröder, *et al.*, "Superchannel engineering of microcombs for optical communications," J. Opt. Soc. Am. B **36**(8), 2013–2022 (2019).
28. T. Lin, A. Dutt, X. Ji, *et al.*, "Broadband high-resolution scanning of soliton micro-combs," in *CLEO: Science and Innovations* (Optica Publishing Group, 2019), paper SF3H–6.
29. J. Riemensberger, A. Lukashchuk, M. Karpov, *et al.*, "Massively parallel coherent laser ranging using a soliton microcomb," Nature **581**(7807), 164–170 (2020).
30. T. Wildi, A. E. Ulanov, T. Voumard, *et al.*, "Phase-stabilised self-injection-locked microcomb," Nat. Commun. **15**(1), 7030 (2024).
31. X. Xue, Y. Xuan, P.-H. Wang, *et al.*, "Normal-dispersion microcombs enabled by controllable mode interactions," Laser Photonics Rev.ews **9**(4), L23–L28 (2015).
32. Ó. B. Helgason, M. Girardi, Z. Ye, *et al.*, "Surpassing the nonlinear conversion efficiency of soliton microcombs," Nat. Photonics **17**(11), 992–999 (2023).
33. J. Liu, H. Tian, E. Lucas, *et al.*, "Monolithic piezoelectric control of soliton microcombs," Nature **583**(7816), 385–390 (2020).
34. J.-Y. Liu, H. Tian, Q.-X. Ji, *et al.*, "Separable integrated frequency control of a microcomb," Optica **12**(9), 1350–1356 (2025).
35. M. Girardi, Ó. B. Helgason, C. H. L. Ortega, *et al.*, "Superefficient microcombs at the wafer level," arXiv (2023).
36. C. Joshi, J. K. Jang, K. Luke, *et al.*, "Thermally controlled comb generation and soliton modelocking in microresonators," Opt. Lett. **41**(11), 2565–2568 (2016).
37. Ó. B. Helgason, F. R. Arteaga-Sierra, Z. Ye, *et al.*, "Dissipative solitons in photonic molecules," Nat. Photonics **15**(4), 305–310 (2021).
38. K. Twayana, Z. Ye, Ó. B. Helgason, *et al.*, "Frequency-comb-calibrated swept-wavelength interferometry," Opt. Express **29**(15), 24363–24372 (2021).
39. P. Del'Haye, S. B. Papp, and S. A. Diddams, "Hybrid electro-optically modulated microcombs," Phys. Rev. Lett. **109**(26), 263901 (2012).
40. E. Lucas, H. Guo, J. D. Jost, *et al.*, "Detuning-dependent properties and dispersion-induced instabilities of temporal dissipative Kerr solitons in optical microresonators," Phys. Rev. A **95**(4), 043822 (2017).
41. S. K. Dacha, Y. Zhao, K. J. McNulty, *et al.*, "Frequency-stable nanophotonic microcavities via integrated thermometry," Nat. Photon. **20**, 71–78 (2026).

Optics EXPRESS

42. Q.-F. Yang, X. Yi, K. Y. Yang, *et al.*, "Spatial-mode-interaction-induced dispersive waves and their active tuning in microresonators," Optica **3**(10), 1132–1135 (2016).
43. X. Yi, Q.-F. Yang, K. Y. Yang, *et al.*, "Theory and measurement of the soliton self-frequency shift and efficiency in optical microcavities," Opt. Lett. **41**(15), 3419–3422 (2016).
44. M. L. Gorodetsky and I. S. Grudinin, "Fundamental thermal fluctuations in microspheres," J. Opt. Soc. Am. B **21**(4), 697–705 (2004).
45. T. E. Drake, J. R. Stone, T. C. Briles, *et al.*, "Thermal decoherence and laser cooling of kerr microresonator solitons," Nat. Photonics **14**(8), 480–485 (2020).
46. B. D. Stone, L. Rukh, G. M. Colación, *et al.*, "Reduction of thermal instability of soliton states in coupled kerr-microresonators," APL Photonics **10**(5), 0257045 (2025).
47. X. Yi, Q.-F. Yang, X. Zhang, *et al.*, "Single-mode dispersive waves and soliton microcomb dynamics," Nat. Commun. **8**(1), 14869 (2017).
48. H. Taheri, A. A. Eftekhar, K. Wiesenfeld, *et al.*, "Soliton formation in whispering-gallery-mode resonators via input phase modulation," IEEE Photonics J. **7**(2), 1–9 (2015).
49. I. Rebolledo-Salgado, C. Quevedo-Galán, Ó. B. Helgason, *et al.*, "Platicon dynamics in photonic molecules," Commun. Phys. **6**(1), 303 (2023).
50. K. Twayana, M. Girardi, and V. Torres-Company, "Quiet point dynamics in photonic molecule microcombs," in *Conference on Lasers and Electro-Optics Europe & European Quantum Electronics Conference* (IEEE, 2025), p. 1.
51. T. Carmon, L. Yang, and K. J. Vahala, "Dynamical thermal behavior and thermal self-stability of microcavities," Opt. Express **12**(20), 4742–4750 (2004).
52. L. Neuhaus, R. Metzdorff, S. Chua, *et al.*, "Pyrpl (python red pitaya lockbox)-an open-source software package for FPGA-controlled quantum optics experiments," in *Conference on Lasers and Electro-Optics Europe & European Quantum Electronics Conference* (IEEE, 2017), p. 1.
53. I. Rebolledo-Salgado, "Raw data for: Continuously tunable super-efficient microcombs," Zenodo: Version 1 (2026), https://doi.org/10.5281/zenodo.18303873.